AFRL-RX-WP-JA-2017-0127

LINEAR AND NONLINEAR OPTICAL RESPONSE IN SILVER NANOCLUSTERS: INSIGHT FROM A COMPUTATIONAL INVESTIGATION (POSTPRINT)

Paul N. Day, Ruth Pachter, and Kiet A. Nguyen

AFRL/RX

Terry P. Bigioni

University of Toledo

11 March 2016
Interim Report

(STINFO COPY)

AIR FORCE RESEARCH LABORATORY
MATERIALS AND MANUFACTURING DIRECTORATE
WRIGHT-PATTERSON AIR FORCE BASE, OH 45433-7750
AIR FORCE MATERIEL COMMAND
UNITED STATES AIR FORCE

REPORT DOCUMENTATION PAGE

Form Approved
OMB No. 0704-0188

1. REPORT DATE *(DD-MM-YY)*	2. REPORT TYPE	3. DATES COVERED *(From - To)*
11 March 2016	Interim	6 May 2010 – 11 February 2016

4. TITLE AND SUBTITLE
LINEAR AND NONLINEAR OPTICAL RESPONSE IN SILVER NANOCLUSTERS: INSIGHT FROM A COMPUTATIONAL INVESTIGATION (POSTPRINT)

5a. CONTRACT NUMBER
IN-HOUSE

5b. GRANT NUMBER

5c. PROGRAM ELEMENT NUMBER

6. AUTHOR(S)
1) Paul N. Day, Ruth Pachter, and Kiet A. Nguyen – AFRL/RX
2) Terry P. Bigioni - University of Toledo
(continued on page 2)

5d. PROJECT NUMBER

5e. TASK NUMBER

5f. WORK UNIT NUMBER
X09X

7. PERFORMING ORGANIZATION NAME(S) AND ADDRESS(ES)
1) AFRL/RX
Wright-Patterson AFB, OH 45433
2) University of Toledo
2801 W Bancroft
Toledo, Ohio 43606
(continued on page 2)

8. PERFORMING ORGANIZATION REPORT NUMBER

9. SPONSORING/MONITORING AGENCY NAME(S) AND ADDRESS(ES)
Air Force Research Laboratory
Materials and Manufacturing Directorate
Wright-Patterson Air Force Base, OH 45433-7750
Air Force Materiel Command
United States Air Force

10. SPONSORING/MONITORING AGENCY ACRONYM(S)
AFRL/RXAP

11. SPONSORING/MONITORING AGENCY REPORT NUMBER(S)
AFRL-RX-WP-JA-2017-0127

12. DISTRIBUTION/AVAILABILITY STATEMENT
Distribution Statement A. Approved for public release: distribution unlimited.

13. SUPPLEMENTARY NOTES
PA Case Number: 88ABW-2016-1007; Clearance Date: 11 Mar 2016. This document contains color. Journal article published in The Journal of Physical Chemistry A, Vol. 120, 5 Jan 2016. © 2016 ACS Publications. The U.S. Government is joint author of the work and has the right to use, modify, reproduce, release, perform, display, or disclose the work.
The final publication is available at pubs.acs.org/JPCA DOI: 10.1021/acs.jpca.5b09623

14. ABSTRACT *(Maximum 200 words)*
We report a density functional theory (DFT) and time-dependent DFT (TDDFT) investigation of the thiolated silver nanoclusters [Ag44(SR)30]4–, Ag14(SR)12(PR′3)8, Ag31(SG)19, Ag32(SG)19, and Ag15(SG)11, which were synthesized and for which one-photon absorption (OPA) characterization is available. Our computational investigation based on careful examination of the exchange-correlation functional used in DFT geometry optimization and for the linear optical properties predictions by TDDFT, demonstrated good agreement with the measured linear absorption spectra, however dependent on the applied functional. Following the benchmarking, we evaluated the two-photon absorption (TPA) response using TDDFT, noting that accurate prediction of OPA is important for suppositions on the spectral range for TPA enhancement because of the sensitivity to the excitation energies. Although the TPA cross-section results are complicated by resonance effects and quantifying TPA cross sections for these systems is difficult, our results indicate that the nanoclusters Ag15 and Ag31/32 are likely to have large TPA cross sections.

15. SUBJECT TERMS
density functional theory (DFT); and time-dependent DFT (TDDFT); thiolated silver nanoclusters; two-photon absorption

16. SECURITY CLASSIFICATION OF:			17. LIMITATION OF ABSTRACT:	18. NUMBER OF PAGES	19a. NAME OF RESPONSIBLE PERSON (Monitor)
a. REPORT	b. ABSTRACT	c. THIS PAGE			Steven Fairchild
Unclassified	Unclassified	Unclassified	SAR	14	19b. TELEPHONE NUMBER *(Include Area Code)* (937) 904-4328

THE JOURNAL OF PHYSICAL CHEMISTRY A

Article

pubs.acs.org/JPCA

Linear and Nonlinear Optical Response in Silver Nanoclusters: Insight from a Computational Investigation

Paul N. Day,[*,†,‡] Ruth Pachter,[*,†] Kiet A. Nguyen,[†,§] and Terry P. Bigioni[∥,⊥]

[†]Air Force Research Laboratory, Materials and Manufacturing Directorate Wright-Patterson Air Force Base, Ohio 45433, United States

[‡]General Dynamics Information Technology, Inc, Dayton Ohio 45431, United States

[§]UES, Inc, Dayton Ohio 45432, United States

[∥]Department of Chemistry and [⊥]The School of Solar and Advanced Renewable Energy, University of Toledo, Toledo, Ohio 43606, United States

Supporting Information

ABSTRACT: We report a density functional theory (DFT) and time-dependent DFT (TDDFT) investigation of the thiolated silver nanoclusters $[Ag_{44}(SR)_{30}]^{4-}$, $Ag_{14}(SR)_{12}(PR'_3)_8$, $Ag_{31}(SG)_{19}$, $Ag_{32}(SG)_{19}$, and $Ag_{15}(SG)_{11}$, which were synthesized and for which one-photon absorption (OPA) characterization is available. Our computational investigation based on careful examination of the exchange-correlation functional used in DFT geometry optimization and for the linear optical properties predictions by TDDFT, demonstrated good agreement with the measured linear absorption spectra, however dependent on the applied functional. Following the benchmarking, we evaluated the two-photon absorption (TPA) response using TDDFT, noting that accurate prediction of OPA is important for suppositions on the spectral range for TPA enhancement because of the sensitivity to the excitation energies. Although the TPA cross-section results are complicated by resonance effects and quantifying TPA cross sections for these systems is difficult, our results indicate that the nanoclusters Ag_{15} and $Ag_{31/32}$ are likely to have large TPA cross sections. The spherical symmetry of the Ag_{44} and Ag_{14} nanoclusters leads to applicability of superatom theory, while it is not as useful for the more oblate geometries of the Ag_{15} and $Ag_{31/32}$ systems.

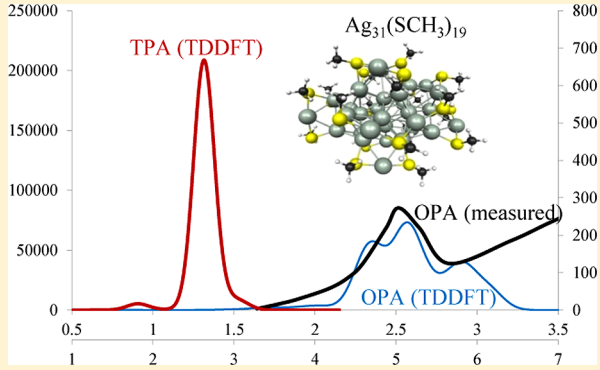

INTRODUCTION

Properties of solution-phase nanoclusters in the size regime of 1−3 nm have drawn significant interest because of increased surface area and changes in the electronic structure as dependent on the bonding structure, among other attributes.[1] Applications ranging from enhanced catalysis, magnetic resonant imaging contrast agents, energy conversion, reduced toxicity, and biological sensing and imaging were investigated. Furthermore, nonlinear optical properties of thiolated gold nanoclusters demonstrated remarkable nonlinear optical enhancements, for example, the two-photon absorption (TPA) cross-section ($\sigma^{(2)}$) (imaginary part of second-order hyperpolarizability) for a thiolated $Au_{25}(SR)_{18}^{-1}$ nanocluster was reported as large as 42 700 GM at 800 nm,[2,3] surpassing TPA cross sections of organic compounds, such as the DANS chromophore, for which $\sigma^{(2)}$ in dimethyl sulfoxide is 191 GM. Very large TPA cross sections were more recently measured for thiolated gold nanoclusters[4−6] and also predicted by calculation.[7] Large static first-order hyperpolarizabilites for thiolate-protected gold nanoclusters were also calculated.[8] At the same time, although optical properties of thiolated silver nanoclusters were found useful in biological applications,[9,10] a theoretical investigation of the nonlinear optical properties of these materials is lacking.

Stable thiolated silver nanoclusters with spherical symmetry such as $[Ag_{44}(SR)_{30}]^{4-}$ and $Ag_{14}(SR)_{12}(PR'_3)_8$ have been synthesized and characterized in the linear optical regime.[11−16] In the experimental work on $[Ag_{44}(SR)_{30}]^{4-}$, the organic group R was either benzoic acid or a fluorinated phenyl group, while for $Ag_{14}(SR)_{12}(PR'_3)_8$, R = $C_6H_3F_2$ and R′ = C_6H_5. These materials tend to follow the superatom number rule, often useful for the prediction and interpretation of the stability and properties of metal nanoclusters. In superatom theory, the valence electrons are assumed to behave as free electrons and, particularly if the system is approximately spherical, will fill electron shells analogous to those in an atom. In a ligated system such as the gold or silver thiolates, the number of valence electrons n^* is given by $n^* = N\nu_A - M - z$, where N is the number of metal atoms, ν_A is the valence of the metal atom (assumed to be 1 for

Received: October 1, 2015
Revised: December 15, 2015
Published: January 5, 2016

DOI: 10.1021/acs.jpca.5b09623
J. Phys. Chem. A 2016, 120, 507−518

gold or silver), M is the number of electron-withdrawing ligands, and z is the net charge of the molecule. For nanoclusters the shell filling order is $1S^2|1P^6|1D^{10}|2S^2 1F^{14}|2P^6 1G^{18}$, yielding magic numbers for stability of 2, 8, 18, 34, 58, etc. (for some systems 20 and 40 may also be part of this sequence).

Recent experimental evidence has shown that stable thiolated gold nanoclusters with less symmetry are not well-described by superatom theory, and indeed a concern has been raised by Joshi et al.[17] regarding the development of a systematic approach to the study of ligand protected metal nanoclusters. Interestingly, while systems with lower symmetry may have less distinct one-photon and two-photon states, there could be the potential for even larger TPA cross sections, similar to the larger TPA cross sections obtained from less symmetrical non-centrosymmetric donor−acceptor systems.[18]

In this work, to assess the nonlinear optical response of silver nanoclusters, we calculated the OPA and TPA properties of $[Ag_{44}(SR)_{30}]^{4-}$ and $Ag_{14}(SR)_{12}(PR'_3)_8$, and for comparison also of the $Ag_{31/32}(SG)_{19}$ and $Ag_{15}(SG)_{11}$ nanoclusters by applying DFT and TDDFT. Synthesis and optical characterization of the silver glutathione nanoclusters $Ag_{32}(SG)_{19}$ and $Ag_{15}(SG)_{11}$ were recently reported by Ashenfelter et al.,[19] while Bertorelle et al.[20] reported experimental results for $Ag_{31}(SG)_{19}$ and $Ag_{15}(SG)_{11}$. In these systems the thiol SG group denotes glutathione, a tripeptide of glutamate, cysteine, and glycine, where the sulfur atom on cysteine bonds to the silver atom. To mitigate issues of incorrect prediction, careful examination of the exchange-correlation functional was undertaken, as used in geometry optimization, as well as for linear and nonlinear optical properties calculations, including GGA, meta-GGA, hybrid, and range-separated hybrid functionals, which we previously benchmarked.[21] We found that while prediction of TPA for these materials is a challenge due to the importance of resonance enhancement and its sensitivity to excitation energies, a larger TPA cross-section for the less symmetrical Ag_{31}/Ag_{32} and Ag_{15} nanoclusters was indicated.

COMPUTATIONAL METHODS

The expression for calculating the TPA cross-section has been previously derived[22−26] (see references therein), given by

$$\delta_{f0}(E_1 + E_2) = \frac{8\pi^4}{(ch)^2} E_1 E_2 g(E_1 + E_2) |S_{f0}(u_1, u_2)|^2 \quad (1)$$

where g is a line width function, $|S_{f0}(u_1,u_2)|^2$ is the two-photon probability corresponding to a transition from the ground-state (0) to a final state (f).

$$|S_{f0}(u_1, u_2)|^2 = \left| \sum_i^N \left[\frac{(\mathbf{u_1} \times \mu_{i0})(\mu_{fi} \times \mathbf{u_2})}{E_i - E_1 + i\Gamma_i} + \frac{(\mathbf{u_2} \times \mu_{i0})(\mu_{fi} \times \mathbf{u_1})}{E_i - E_2 + i\Gamma_i} \right] \right|^2 \quad (2)$$

where E_1 and E_2 are the energies of the two photons with unit polarization vectors $\mathbf{u_1}$ and $\mathbf{u_2}$, respectively. The transition dipole moments are given by μ_{ij}, the state energies by E_i, and the state decay constants by Γ_i.

Each term in the sum-over-states (SOS) in Equation 2 involves three states (ground-state, final-state, and the intermediate-state over which the sum is carried), and in the essential three-state model, the assumption is that a single term dominates in the SOS. In some cases, the TPA cross-section can be estimated accurately by this approximation. This is particularly true in centrosymmetric systems because the terms involving the dipole moments are zero, and a more limited number of state transitions are dipole-allowed. For example, in a system with C_{2h} symmetry, the ground state has A_g symmetry, the strongly allowed OPA states are of B_u symmetry, and the strong TPA states are A_g. In the three-state approximation for the case where the two photons have the same energy (E_λ), the cross-section is given by

$$\delta_{f0}^I = \frac{32\pi^4 g_{max}}{15(ch)^2} \frac{E_\lambda^2}{(E_i - E_\lambda)^2} |\mu_{0i}|^2 |\mu_{if}|^2 (2\cos^2 \Theta_{\mu\mu} + 1) \quad (3)$$

where g_{max} is the maximum of the line width function, and $\Theta_{\mu\mu}$ is the angle between the two transition dipole moment vectors. While the three-state approximation is often not adequate for quantitative results, it can be useful in analyzing the origin of the TPA intensity, as we have previously shown.[26] As we have discussed previously,[7] the TPA probability expressed in Equation 2 can be obtained directly from the residue of the quadratic response, providing a more efficient method for calculating TPA cross sections. Because of the size of the clusters studied in the paper, this is the method we used to calculate the TPA cross sections. This method has the disadvantage of not having the damping factor Γ_i, which can be useful for mitigating unphysically large values near resonances. This damping factor represents the line width of the virtual state i, and when used has typically been set to a small value such as 0.05 eV. While this factor generally has little effect on the TPA cross-section for organic systems, the higher density of states in the metal cluster systems makes near-resonance conditions more likely, and the inclusion of an accurate damping factor may dampen the enhancement, although it is still expected to occur.

Crystal structures for $[Ag_{44}(SR)_{30}^{4-}]$[11,12] and $[Ag_{14}(SR)_{12}(PR'_3)_8]$[15] were used as starting points for geometry optimizations using DFT. The $Ag_{44}(SH)_{30}^{4-}$ system was optimized using the BP86[27,28] exchange-correlation (X-C) functional with the zero-order regular approximation (ZORA) TZP basis set[29] in ADF.[30,31] The $Ag_{14}(SR)_{12}(PR'_3)_8$ system was optimized with the PW91[32] GGA functional using ZORA-TZP[29] in ADF,[30,31] as well as with the GGA PBE[33] and hybrid PBE0[34] (X-C) functionals and the LANL2DZ basis set[35] in Gaussian 09.[36] The starting structures used for the Ag_{31}/Ag_{32} and Ag_{15} systems are discussed in the Results and Discussion section. The Ag_{32} system has an odd number of electrons, and the ground state is a doublet; spin-unrestricted DFT was used in this case. DFT optimizations using the hybrid B3LYP[27,37−40] and PBE0[34] functionals were performed with the LANL2DZ basis set[35] in Gaussian 09.[36] OPA spectra were calculated using linear response TDDFT in the programs ADF,[26,27] Gaussian 09,[36] GAMESS,[41] and Dalton.[42] Dalton was used to calculate TPA spectra within quadratic response TDDFT. The LB94[43] functional based on an improved model of the potential, presumably taking into account the asymptotic behavior, and an improved version SAOP,[44] as well as the PBE,[33] PBE0,[34] M06,[45] B3LYP, and the hybrid range-separated CAMB3LYP[46] and mCAMB3LYP[47] (X-C) functionals were used in the TDDFT calculations with the ZORA-TZP,[29] LANL2DZ,[35] and SDD[48,49] basis sets. The polarizable continuum model (PCM)[50] was used to include solvent effects where indicated.

RESULTS AND DISCUSSION

Ag_{44}. The structure and linear absorption spectra in the $[Ag_{44}(SR)_{30}]^{4-}$ nanocluster were reported by Desireddy et al.,[11,12] and experimental and PBE spectra were also reported by Yang et al.[13] The experimental linear absorption peaks are at nearly the same wavelength whether the ligand (R) is

DOI: 10.1021/acs.jpca.5b09623
J. Phys. Chem. A 2016, 120, 507−518

p-mercaptobenzoic acid or any of three fluorinated arylthiols (SPhF, $SPhF_2$, and $SPhCF_3$), and a simplified system was used in our calculations, with R = H and D_{2h} symmetry enforced, as shown in Figure 1. The geometry was optimized with several

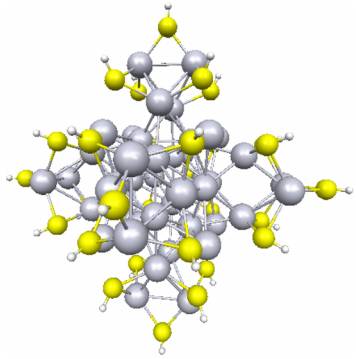

Figure 1. Optimized structure of $Ag_{44}(SR)_{30}^{4-}$ (R = H; see text for details).

functionals, using the Desireddy et al.[11] structure as a guide. The BP86 functional provided the best agreement with experiment; thus, this optimized structure was used in the TDDFT calculations.

The structure of the nanocluster consists of a hollow icosahedral core of 12 silver atoms surrounded by 20 silver atoms in the form of a dodecahedron, with each of these 20 atoms centered above one of the 20 triangular faces of the core icosahedron, maintaining the I_h symmetry. This structure is surrounded by 24 sulfur atoms in an approximate rhombicuboctahedral (RCO) arrangement. As this structure has O_h symmetry, this reduces the symmetry of the structure to T_h. The structure is completed with six Ag_2S caps on six faces of the RCO, which maintains the approximate T_h structure. Alternative views of the structure could have Ag_2S_5 capping structures or Ag_4S_5 capping structures, where in the latter view, two of the silver atoms have been extracted from the dodecahedron for each cap, and the remaining eight silver atoms in the dodecahedron form a cube that encases the core icosahedron, yielding an alternative Ag_{20}^{2+} core.[11] While this view of the structure involves the smallest formal charges, the cubic core was found to have no highest occupied molecular orbital−lowest unoccupied molecular orbital (HOMO−LUMO) gap. In the case of the Ag_2S_5 capping structures, however, a large HOMO−LUMO gap was found for the approximately spherical Ag_{32}^{14+} core. On the basis of this analysis of the electronic structure for the two alternative views, it was concluded that the correct view of the capping structures was Ag_2S_5 mounts.[11]

In our calculations at the BP86//TZP-ZORA level of theory (see Computational Methods section), the silver atoms that would be extracted from the dodecahedron to form Ag_4S_5 caps have strong, short bonds (2.98 Å) to the inner icosahedral silver atoms, and weaker longer bonds (3.33 Å) to the outer Ag atoms, indicating that the preferable view is indeed that of Ag_2S_5 as capping structures and the dodecahedral silver atoms as providing sturdy mounts. Also, each of the RCO sulfur atoms is bonded to three silver atoms, with the strongest and shortest bond (2.56 Å) to the outer Ag, the intermediate length bond (2.65 Å) to the mounting Ag, and the weakest and longest bond (2.71 Å) to the corner Ag, further supporting the view of Ag_2S_5 caps. The outermost sulfur atoms each have just two bonds, and these are to the outer Ag atoms and are similar in length (2.56 Å) to the other Ag−S bonds in the capping structure. $[Ag_{44}(SR^{30})]^{4-}$ crystal structures reported by Yang et al.[13] have the same qualitative features that support a model with Ag_2S_5 caps. When R = PhF, the bond lengths between the RCO sulfur atoms and the Ag atoms have the same ordering: 2.538 Å (to outer Ag atoms), less than 2.559 Å (to mount Ag atoms), and less than 2.638 Å (to corner Ag atoms), although the differences are not as large as in our calculations.

The excitation energies of the first five peaks in the spectrum, including measured results and those calculated with six different functionals, as well as the mean unsigned errors (MUEs) relative to measurement, are listed in Table 1. The superatom theory's

Table 1. Linear Absorption Data[a] for $Ag_{44}(SR)_{30}^{4-}$

	peak1	peak2	peak3	peak4	peak5	MUE
PBE/ZORA:TZP	1.163	1.858	2.263	2.978	3.308	0.245
LB94/ZORA:TZP	1.311	1.851	2.191	2.431	3.066	0.106
SAOP/ZORA:TZP	1.301	1.911	2.261	2.451	3.096	0.084
B3LYP/LANL2DZ	1.414	1.914	2.279	2.619	2.894	0.057
CAMB3LYP/LANL2DZ	1.386	2.076	2.536	2.921	3.161	0.216
mCAM/LANL2DZ	1.373	1.948	2.358	2.688	3.058	0.090
PBE[13]	1.300	1.931	2.210	2.480	2.980	0.066
measured[13]	1.488	1.934	2.317	2.567	3.017	0.026
measured[11]	1.483	1.921	2.304	2.513	2.972	0.000

[a]In electronvolts. Geometry optimized using BP86/ZORA:TZP and fwhm = 0.2 eV.

so-called magic number n^* for this system is 18, filling the superatomic orbitals $1S^2|1P^6|1D^{10}$. The lowest-energy excitations are dominated by transitions of 1D electrons to the unfilled 2S and 1F superatomic orbitals. This large number of delocalized electrons, combined with the inner shell of silver atoms, which is isolated from the effects of the thiolate ligands, allows for a number of low energy transitions. In the TDDFT calculations, the first peak in the spectrum falls in the range of 1.30−1.41 eV, just below the measured value of 1.48 eV. The B3LYP functional performed best overall, with a MUE of 0.057 eV. Note that these values are lower than those previously calculated with PBE.[13] The OPA spectrum calculated with B3LYP is compared to the measured spectrum in Figure 2, and in Figure S1 in Supporting Information, where spectra calculated using other functionals are also included. The B3LYP functional was thus used to calculate the TPA for the first 100 TPA-allowed states, which extends to ∼2.9 eV. The calculated TPA spectrum is shown in Figure 3 along with the corresponding OPA.

The resonance enhancement factor τ for TPA is defined by $\tau = \left(\frac{E_i}{E_f} - 0.5\right)^{-2}$. Thus, the calculated TPA peak at 2.75 eV (corresponding to two 901 nm photons) is the result of resonance enhancement from the states that contribute to the first OPA peak at 1.33 eV (934 nm; see Figure 3). Three degenerate states of B_{1u}, B_{2u} and B_{3u} symmetries at an excitation energy of 1.3276 eV, each with an oscillator strength of 0.0179, cause enhancement of two-photon-allowed states in the energy range of 2.5−2.8 eV, particularly those of A_g symmetry, which give the largest contribution to the TPA cross-section. The trios of degenerate OPA states at 1.8377 and 2.1865 eV are expected to cause significant TPA enhancement near 3.68 and 4.37 eV, respectively, but our TPA calculation does not extend to that energy, as this spectral region is of less interest for application. In Figure S2 we show a plot of τ versus the transition energy.

DOI: 10.1021/acs.jpca.5b09623
J. Phys. Chem. A 2016, 120, 507−518

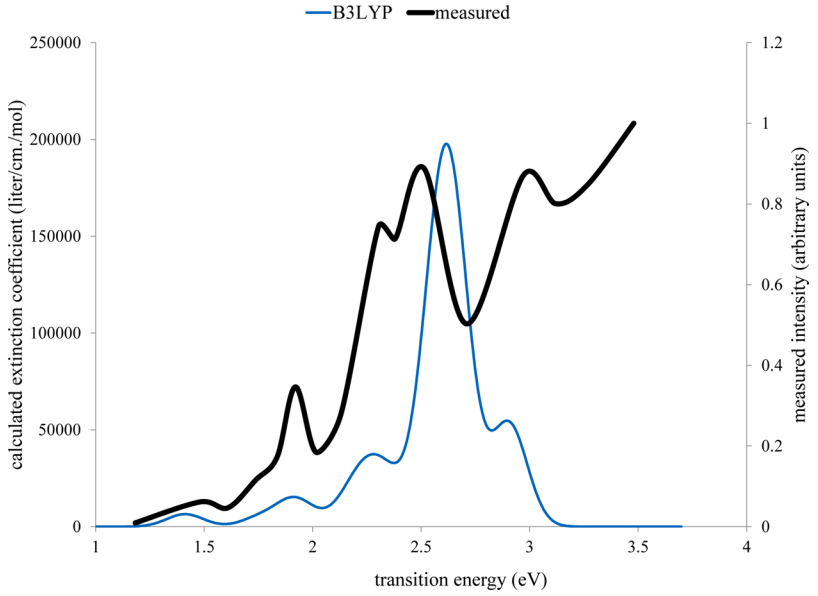

Figure 2. Linear absorption spectrum of $Ag_{44}(SR)_{30}^{4-}$. Calculated spectra for SR = SH and a line width of 0.2 eV, while the measured spectrum of Desireddy et al.[11] had SR = *p*-mercaptobenzoic acid.

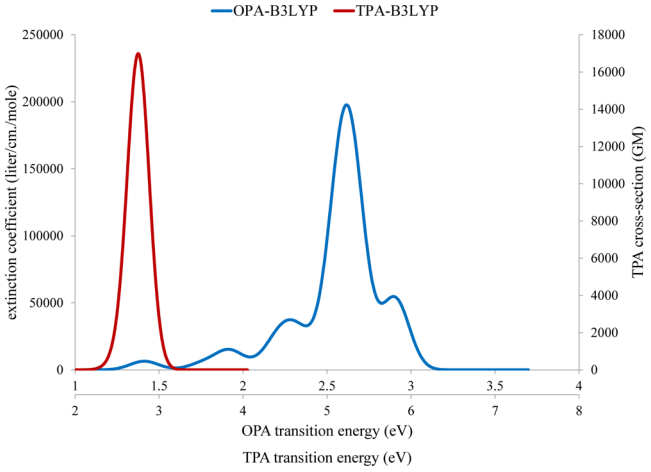

Figure 3. OPA and TPA spectra of $Ag_{44}(SR)_{30}^{4-}$ using the B3LYP functional, with the TPA transition energies plotted double scale of the OPA transition energies, to show the relationship between the states causing the resonance enhancement.

As expected, the TPA states near the resonance transition energy of 2.66 eV have a large enhancement. Calculated TPA cross sections for each TPA-allowed state versus the resonance enhancement factor τ for that state (see Figure 4) demonstrate that the resonance enhancement is an important factor in the TPA cross section for the silver nanocluster. Interestingly, although the five states with the largest TPA cross section also have large resonant enhancement factors, the states with the highest resonant enhancement of 13 277, a trio of states at 2.702 eV, have relatively small TPA cross sections. A number of other states with large resonance enhancement factors have insignificant contributions to the TPA. Thus, while the resonance enhancement factor is important, it is just one factor in determining the TPA cross-section, along with the ground-state and excited-state transition dipole moments.

Ag_{14}. The crystal structure and linear absorption spectrum of the thiolated silver nanocluster $Ag_{14}(SR)_{12}(PR'_3)_8$ has been reported by Yang et al.[15] (R = $C_6H_3F_2$ and R′ = phenyl), and Gell et al.[16] performed some computational analysis of this system. Additional studies were performed by Muniz-Miranda et al.[51] and Goh et al.,[52] which have mentioned that this structure satisfies the superatom nanocluster criteria. The optimized structures are shown in Figure 5.

The core of the $Ag_{14}(SR)_{12}(PR'_3)_8$ nanocluster structure is comprised of six silver atoms located at the vertices of an icosahedron. The remaining eight silver atoms are located at the corners of a cube that surrounds the icosahedron. The 12 sulfur atoms are located near the center of each of the 12 edges of this cube but are distorted so as to bond with only one of the core icosahedral silver atoms, while bonding with two of the corner atoms. The sulfur atom's bond to the core silver atom is the shorter, stronger bond, with an average bond length of 2.54 Å in the crystal structure, compared to 2.65 Å for the outer Ag−S bonds. Table S1 in Supporting Information lists the bond lengths for this structure with different ligands, including the reported crystal structure,[15] the PBE optimized structure of Gell, at al.,[16] and our optimized structures using the PBE, PBE0, and PW91 X-C functionals. While the lowest structural errors were obtained when the ligands were replaced with methyl groups and either the PBE/VASP or the PW91/IMCP-SR1 level of theory was used, the structures with just methyl groups did not yield accurate spectra in the TDDFT calculations (see Table 2).

The measured linear absorption spectrum,[15] shown in Figure 6 and listed in Table 2, has a small peak at 2.34 eV (530 nm) and a sharper, more intense peak at 3.37 eV (368 nm). The nanocluster's smaller size compared to $[Ag_{44}(SR^{30})]^{4-}$ causes more quantum confinement, leading to larger transition energies and a more blue-shifted spectrum. When methyl groups are used as ligands, the calculated spectrum using TDDFT is too blue-shifted, but when the C_6H_4F group is used as the sulfur ligand, good agreement with experiment is obtained using the LB94 functional, and fair agreement is obtained using the SAOP functional. The results using the B3LYP, PBE0, CAMB3LYP, and M06 X-C functionals are still too blue-shifted. Note that the superatom magic number for $Ag_{14}(SR)_{12}(PR'_3)_8$ is 2, corresponding to the filling of the 1S superatom orbital.

DOI: 10.1021/acs.jpca.5b09623
J. Phys. Chem. A 2016, 120, 507−518

Figure 4. Calculated TPA cross-section of $Ag_{44}(SR)_{30}^{4-}$ for each TPA-allowed state vs its resonance enhancement factor.

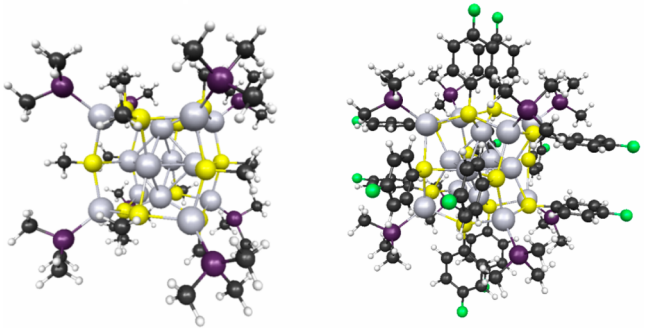

Figure 5. Optimized structures for $Ag_{14}(SCH_3)_{12}(P(CH_3)_3)_8$ and $Ag_{14}(SC_6H_5F)_{12}(P(CH_3)_3)_8$ (see text for details).

The TPA for this system was calculated with methyl ligands using the B3LYP and CAMB3LYP functionals. When the B3LYP X-C functional was used, a peak TPA of ~40 GM was obtained at a transition energy of ~4.1 eV (corresponding to two 605 nm photons). When the CAMB3LYP functional is used, the calculated peak intensity is only ~20 GM, and it is blue-shifted by ~0.7 eV (not shown). A blue shift in the excitation energy when using the range-separated hybrid functional CAMB3LYP versus hybrid B3LYP has been previously explained.[21] The TPA and OPA spectra calculated with the CAMB3LYP functional are plotted in Figure 7. The calculated TPA for this system is less (by a factor of ~400) than was calculated for the nanocluster with 44 silver atoms. The strong TPA is in the range of 4−5 eV, but since there are no OPA states in the 2.0−2.5 eV range (the OPA states are above 3.0 eV), the resonance enhancement factor is small, and the TPA cross-section is small. Note that a large resonance enhancement occurs when the excitation energy of an OPA state is close to half that of a TPA state. Because all the OPA states for the Ag_{14} system are significantly higher in energy than half the TPA energy over the range we are investigating, all the enhancement factors in the TPA range of interest are less than 20.

Table 2. Linear Absorption Spectra for $Ag_{14}(SR)_{12}(PR'_3)_8$ (eV)

R	R′	geometry	TDDFT	MUE	err1	err2	point1	point2
CH_3	CH_3	PW91	LB94/ZORA:TZP	0.26	0.41	−0.11	2.75	3.26
CH_3	CH_3	PW91	SAOP/ZORA:TZP	0.69	0.62	0.76	2.96	4.13
CH_3	CH_3	PBE	PBE/ZORA:TZP	0.72	0.87	0.57	3.20	3.94
CH_3	CH_3	PBE	LB94/ZORA:TZP	0.62	0.74	0.50	3.07	3.86
CH_3	CH_3	PBE	SAOP/ZORA:TZP	0.21	0.41	−0.01	2.75	3.36
CH_3	CH_3	PBE	CAMB3LYP/SDD	1.48	1.26	1.70	3.60	5.07
C_6H_4F	CH_3	PBE	LB94/ZORA:TZP	0.03	0.00	−0.07	2.34	3.30
C_6H_4F	CH_3	PBE	SAOP/ZORA:TZP	0.12	0.16	0.08	2.49	3.44
C_6H_4F	CH_3	PBE	B3LYP/SDD	0.64	0.73	0.54	3.07	3.91
C_6H_4F	CH_3	PBE	CAMB3LYP/SDD	1.48	1.26	1.70	3.60	5.07
C_6H_4F	CH_3	PBE	M06/LANL2DZ	0.72	0.74	0.71	3.08	4.08
C_6H_4F	CH_3	PBE0	PBE0/LANL2DZ	1.04	0.90	1.17	3.24	4.54
C_6H_4F	CH_3	PBE0	LB94/ZORA:TZP	0.06	0.02	−0.10	2.36	3.27
C_6H_4F	CH_3	PBE0	SAOP/ZORA:TZP	0.10	0.17	−0.04	2.50	3.32
C_6H_4F	CH_3	PBE0	B3LYP/LANL2DZ	0.83	0.78	0.87	3.12	4.24
C_6H_4F	CH_3	PBE0	CAMB3LYP/SDD	1.58	1.33	1.82	3.67	5.19
C_6H_4F	CH_3	PBE0	M06/LANL2DZ	0.80	0.74	0.86	3.08	4.23
$C_6H_3F_2$	phenyl		measured[15]				2.34	3.37

DOI: 10.1021/acs.jpca.5b09623
J. Phys. Chem. A 2016, 120, 507−518

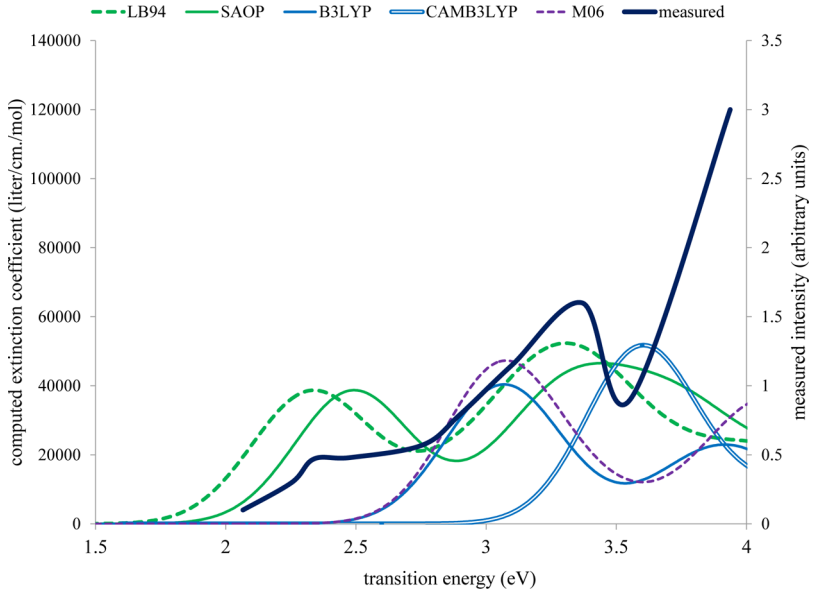

Figure 6. Linear absorption of $Ag_{14}(SR)_{12}(PR'_3)_8$. For calculated spectra, R = C_6H_4F, R′ = CH_3, the geometry was optimized with the PBE functional, and the line width is 0.5 eV. For the measured data from Yang, et al.,[15] R = $C_6H_3F_2$ and R′ = phenol.

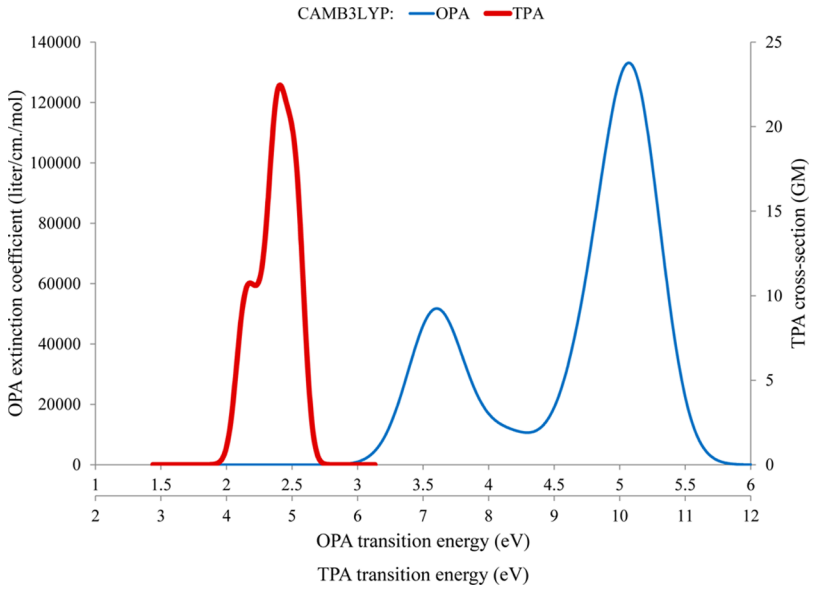

Figure 7. OPA and TPA spectra of $Ag_{14}(SR)_{12}(PR'_3)_8$, with the TPA transition energies plotted double scale of the OPA transition energies. R = R′ = methyl.

Ag_{31}/Ag_{32} and Ag_{15}. Synthesis and optical characterization of the $Ag_{32}(SG)_{19}$, $Ag_{31}(SG)_{19}$, and $Ag_{15}(SG)_{11}$ silver glutathione nanoclusters have been reported.[19,20] A structure for $Ag_{15}(SG)_{11}$ consisting of an Ag_8 core protected by two L1 ligands, one L2 ligand, and one L3 ligand (L1, L2, and L3, have structures of −S(G)−Ag−S(G)−, −S(G)−Ag−S(G)−Ag−S(G)−, and −S(G)−Ag−S(G)−Ag−S(G)−Ag−S(G)−, respectively) was proposed.[20] A structure was also proposed[20] for $Ag_{31}(SG)_{19}$ consisting of an Ag_{21} core protected by eight L1 ligands and one L2 ligand. We propose a similar structure for $Ag_{32}(SG)_{19}$, where two of the L1 ligands are connected by the additional Ag atom to form an L3 ligand, resulting in a structure with six L1 ligands, one L2 ligand, and one L3 ligand. The geometries for these systems, with SCH_3 replacing SG, were optimized using the B3LYP functional and LANL2DZ basis set (see Computational methods section). Both gas-phase and aqueous (using PCM to include the solvent effect) geometries were obtained, and the solution-phase geometries are shown in Figure 8. The coordinates for these aqueous systems optimized with the PBE0 functional are listed in Table S2.

Figure 9 and Tables 3 and 4 show the measured and calculated linear absorption spectra for the Ag_{31}/Ag_{32} systems. The measured linear absorption spectrum of the material that Bertorelle et al.[20] report to be $Ag_{31}(SG)_{19}$ has a sharp peak at 2.52 eV, while a measured peak centered at 2.59 eV is shown in spectra by Kumar et al.,[53] as well as by Ashenfelter et al.,[19] labeled "band 6", and identified as the nanocluster $Ag_{32}(SG)_{19}$. In the TDDFT calculations of Bertorelle et al.,[20] where the SG ligands were replaced by SCH_3, they obtained a peak at 2.42 eV, using CAMB3LYP in the gas-phase. Note that neutral $Ag_{31}(SG)_{19}$ and $Ag_{32}(SG)_{19}$ have free electron counts of 12 and 13, respectively, which are not magic numbers. If $Ag_{31}(SG)_{19}$ had a charge of

DOI: 10.1021/acs.jpca.5b09623
J. Phys. Chem. A 2016, 120, 507−518

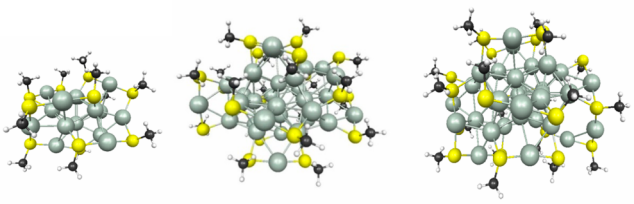

Figure 8. Solution-phase optimized structures for $Ag_{15}(SCH_3)_{11}$, $Ag_{31}(SCH_3)_{19}$, and $Ag_{32}(SCH_3)_{19}$.

either +4 or −6 (+5 or −5 for $Ag_{32}(SG)_{19}$), it would have a "superatom" free electron count of 8 or 18, which are both magic numbers. However, attempts to optimize $Ag_{31}(SG)_{19}$ with charges +4 and −6 were not successful, and a minimum energy structure has been found only for the neutral system. The $Ag_{32}(SG)_{19}$ structure was also optimized with zero charge, and since this system has an odd number of electrons, spin-unrestricted DFT was used. Because these structures do not have the spherical symmetry of the Ag_{44} and Ag_{14} systems, the superatom magic number theory may be less applicable.

As can be seen in Figure 9, when the linear absorption spectrum is calculated using the CAMB3LYP functional and PCM solvation model, excellent agreement is obtained with this measured peak for both $Ag_{31}(SCH_3)_{19}$ (peak at 2.52 eV) and $Ag_{32}(SCH_3)_{19}$ (peak at 2.49 eV), assuming a peak full-width at half-maximum (fwhm) of 0.2 eV for all calculated states below 2.7 eV. For higher energy states, a fwhm of 0.5 eV was used to obtain better agreement with experiment in this part of the spectrum. As can be seen by the results listed in Tables 3 and 4, good agreement is obtained whenever the CAMB3LYP functional is used, whether or not the PCM solvation model is included, while when the B3LYP, PBE0, or mCAMB3LYP functionals were used, the peak is significantly red-shifted. While the good agreement of the calculated results with measurements gives credence to the structures and methods used, the similarity of the absorption spectra for $Ag_{31}(SG)_{19}$ and $Ag_{32}(SG)_{19}$ in both the measured and calculated results means they cannot be used to distinguish between the two structures.

Table 3. Linear Absorption Spectra for $Ag_{31}(SR)_{19}$ (eV)

geometry	TDDFT	error	peak
PBE0/ZORA:TZP	CAMB3LYP/LANL2DZ	−0.115	2.400
B3LYP/LANL2DZ	PBE0/LANL2DZ	−0.259	2.256
B3LYP/LANL2DZ	B3LYP/LANL2DZ	−0.345	2.170
B3LYP/LANL2DZ	CAMB3LYP/LANL2DZ	0.072	2.587
B3LYP/LANL2DZ	CAMB3LYP/ LANL2DZ(PCM)	0.026	2.541
B3LYP/LANL2DZ(PCM)	PBE0/LANL2DZ(PCM)	−0.250	2.265
B3LYP/LANL2DZ(PCM)	B3LYP/LANL2DZ(PCM)	−0.261	2.255
B3LYP/LANL2DZ(PCM)	CAMB3LYP/ LANL2DZ(PCM)	0.008	2.523
PBE0/LANL2DZ	PBE0/LANL2DZ	−0.274	2.241
PBE0/LANL2DZ	B3LYP/LANL2DZ	−0.345	2.170
PBE0/LANL2DZ	CAMB3LYP/LANL2DZ	0.056	2.571
PBE0/LANL2DZ(PCM)	PBE0/LANL2DZ(PCM)	−0.244	2.271
PBE0/LANL2DZ(PCM)	B3LYP/LANL2DZ(PCM)	−0.291	2.224
PBE0/LANL2DZ(PCM)	CAMB3LYP/ LANL2DZ(PCM)	−0.028	2.487
PBE0/LANL2DZ(PCM)	mCAMB3LYP/ LANL2DZ(PCM)	−0.199	2.316
	measured[20]		2.515

The TPA for $Ag_{31}(SCH_3)_{19}$ was calculated at the CAM-B3LYP//PBE0 level of theory and plotted in Figure 10, along with the OPA at the same level of theory. The TPA transition energies are plotted double scale to aid in noticing resonance effects. As the oscillator strengths for the first three excited states are small (S_1 = 0.89 eV, f = 0.001; S_2 = 1.31 eV, f = 0.001; S_3 = 1.50 eV, f = 0.004), the correspondence is not easily observed in this plot. However, in Figure S3, the TPA from each final state is plotted versus the resonance enhancement factor τ using each of the first three OPA states as the intermediate state. This plot shows that the TPA peak near 2.62 eV of 668 GM is the result of two final states with contributions of 458 GM and 187 GM that benefit from large resonance enhancement factors of 1 000 000 and 400 000 due to S_2. One can also observe that the small TPA peak of 17 GM near 1.9 eV is the result of resonance enhancement with S_1 producing a factor of τ = 31 000. Currently we were able to perform TPA calculations on this system for the

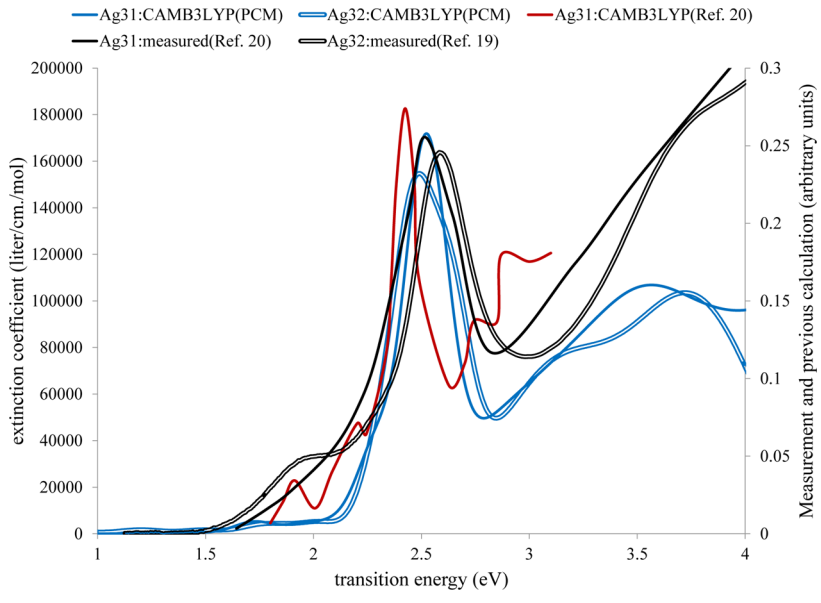

Figure 9. OPA spectra for Ag_{31}/Ag_{32} nanoclusters.

DOI: 10.1021/acs.jpca.5b09623
J. Phys. Chem. A 2016, 120, 507−518

Table 4. Linear Absorption Spectra for $Ag_{32}(SR)_{19}$ (eV)

geometry	TDDFT	error	peak
B3LYP/LANL2DZ(PCM)	CAMB3LYP/LANL2DZ(PCM)	−0.095	2.488
PBE0/LANL2DZ	PBE0/LANL2DZ	−0.451	2.132
PBE0/LANL2DZ	B3LYP/LANL2DZ	−0.546	2.037
PBE0/LANL2DZ	CAMB3LYP/LANL2DZ	−0.097	2.486
PBE0/LANL2DZ	mCAMB3LYP/LANL2DZ	−0.338	2.245
PBE0/LANL2DZ(PCM)	PBE0/LANL2DZ(PCM)	−0.259	2.324
PBE0/LANL2DZ(PCM)	B3LYP/LANL2DZ(PCM)	−0.329	2.254
PBE0/LANL2DZ(PCM)	mCAMB3LYP/LANL2DZ(PCM)	−0.182	2.401
	measured[19]		2.583

first 30 states, extending to 3.1 eV, but we expect that much larger TPA cross sections will be obtained at transition energies greater than 4.0 eV due to resonance enhancement with the stronger OPA states in the range of 2.3−2.6 eV.

The measured and calculated linear absorption spectrum for $Ag_{15}(SR)_{11}$ is given in Table 5. Figure 11 compares spectra computed with the PBE0 functional to the measured data, while Figure S4 includes calculated data using additional functionals. The experimental linear absorption spectra reported for $Ag_{15}(SG)_{11}$[19,20] are distinguished by a steep rise between 2.2 and 2.5 eV followed by a flat plateau from 2.6 to 3.2 eV. The theoretical spectrum previously reported by Bertorelle et al.[20] has a narrow peak at 2.17 eV, another peak at 2.85 eV, and a more intense narrow band at 3.02 eV, and correspondence with measurement is not apparent. According to superatom theory, with a neutral charge this system has four free electrons, which is not a magic number for stability. In our calculations, both the neutral system and the cation with a charge of +2, a system for which the number of free electrons is the magic number 2, were optimized. However, spectra calculated from the cation are not in as good agreement with measurement, and we focus on the neutral system in the following. As with the Ag_{31} nanocluster, Ag_{15} is not spherically symmetrical, and superatom theory may not be applicable. Our calculated spectra in Figure 11 use a line width of 0.5 eV and include both gas-phase and aqueous results, using the PCM solvation model.

The most distinguishing feature in the absorption spectra for $Ag_{15}(SG)_{11}$[19,20] is the steep rise near 2 eV. To quantify this feature, we analyzed the first derivative of the absorption intensity with respect to the excitation energy, and the maximum in this derivative indicates the energy where the rise is the steepest. This normalized derivative (ND) is also listed in Table 5. The results demonstrate that, while several calculations both with and without PCM show good agreement with experiment (i.e., absolute error less than 0.100 eV), when PCM is not used the rise is not steep enough, so the shape of the plot is not in such good agreement with experiment (see Figure 11). Overall, the solvated results are in better agreement with experiment, particularly when the PBE0 functional is used for TDDFT calculations. Fair results were obtained with the B3LYP and mCAMB3LYP functionals, while the solvated CAMB3LYP results are not in as good agreement with experiment due to a 0.2 eV blue shift of the strong excited state relative to the mCAMB3LYP calculation.

Figure 12 shows the calculated TPA spectra using the CAMB3LYP functional and two different geometries (from B3LYP and PBE0 optimizations). Despite the similarities in the two functionals as well as in the resulting structures, the sensitivity of the excitation energies to structure and of the TPA cross sections to resonance effects results in different TPA spectra. Calculated OPA spectra are also shown for these two levels of theory, plotted at half-scale to illustrate how the single photon resonances contribute to the calculated TPA. When the B3LYP geometry is used, the first excited state at 1.85 eV is in resonance with several states near 3.7 eV, resulting in an extremely large calculated TPA of over 60 000 GM. When the PBE0 functional is used, the first excited state is at 1.27 eV, but since no calculated states are particularly close in energy to 2.54 eV, there is not a large TPA resonance effect from this state. However, the second excited state near 2.11 eV is in resonance with several states near 4.22 eV, and therefore this calculation produces a large TPA at this energy. This is further illustrated in Figure S5, where the TPA cross-section for each final state using the CAMB3LYP//PBE0 level of theory is plotted versus the resonance enhancement factor τ, which has been calculated using

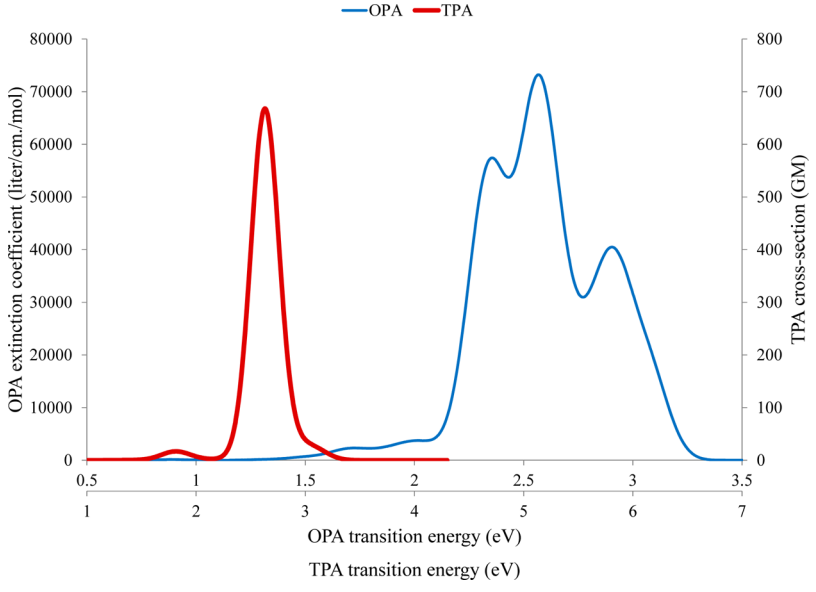

Figure 10. OPA and TPA spectra of $Ag_{31}(SR)_{19}$, with the TPA transition energies plotted double scale of the OPA transition energies. The line width is 0.2 eV for OPA and 0.3 eV for TPA.

DOI: 10.1021/acs.jpca.5b09623
J. Phys. Chem. A 2016, 120, 507−518

Table 5. Linear Absorption Spectra[a] for $Ag_{15}(SR)_{11}$

geometry	TDDFT	TE	error	ND
B3LYP/LANL2DZ	SAOP/ZORA:TZP	2.077	−0.262	2.56
B3LYP/LANL2DZ	LB94/ZORA:TZP	1.973	−0.367	2.67
B3LYP/LANL2DZ	PBE0/LANL2DZ	2.298	−0.042	3.62
B3LYP/LANL2DZ	B3LYP/LANL2DZ	2.207	−0.132	3.41
B3LYP/LANL2DZ	CAMB3LYP/LANL2DZ	2.657	0.318	3.63
B3LYP/LANL2DZ	CAMB3LYP/SDD	2.606	0.266	3.10
B3LYP/LANL2DZ	CAMB3LYP/SDD	2.576	0.236	3.29
B3LYP/LANL2DZ	mCAMB3LYP/LANL2DZ	2.382	0.043	3.72
PBE0/LANL2DZ	SAOP/ZORA:TZP	2.010	−0.329	2.74
PBE0/LANL2DZ	LB94/ZORA:TZP	1.982	−0.357	2.64
PBE0/LANL2DZ	PBE0/LANL2DZ	2.391	0.052	2.39
PBE0/LANL2DZ	B3LYP/LANL2DZ	2.306	−0.033	2.57
PBE0/LANL2DZ	CAMB3LYP/LANL2DZ	2.455	0.116	2.67
PBE0/LANL2DZ	CAMB3LYP/SDD	2.340	0.000	2.83
PBE0/LANL2DZ	mCAMB3LYP/LANL2DZ	2.450	0.111	2.08
B3LYP/LANL2DZ(PCM)	PBE0/LANL2DZ(PCM)	2.317	−0.022	3.87
B3LYP/LANL2DZ(PCM)	B3LYP/LANL2DZ(PCM)	2.212	−0.127	4.17
B3LYP/LANL2DZ(PCM)	CAMB3LYP/ LANL2DZ(PCM)	2.653	0.313	3.90
B3LYP/LANL2DZ(PCM)	mCAMB3LYP/ LANL2DZ(PCM)	2.404	0.065	4.17
PBE0/LANL2DZ(PCM)	PBE0/LANL2DZ(PCM)	2.370	0.030	3.96
PBE0/LANL2DZ(PCM)	B3LYP/LANL2DZ(PCM)	2.274	−0.065	3.87
PBE0/LANL2DZ(PCM)	CAMB3LYP/ LANL2DZ(PCM)	2.717	0.378	3.95
PBE0/LANL2DZ(PCM)	CAMB3LYP/SDD(PCM)	2.440	0.101	3.03
PBE0/LANL2DZ(PCM)	mCAMB3LYP/ LANL2DZ(PCM)	2.464	0.125	3.98
PBE0/LANL2DZ(PCM)	mCAMB3LYP/SDD(PCM)	2.279	−0.060	2.44
	measured(Bertorelle et al.)[20]	2.458	0.119	4.92
	measured(Ashenfelter et al.)[19]	2.339	0.000	5.90

[a]Transition energy (TE in units of eV) where the derivative of the intensity with respect to the TE is a maximum, as well as the error (eV) compared to measurement. The normalized derivative (ND) of the intensity has units of $(eV)^{-1}$.

each of these first two excited states as the intermediate state. For the final states contributing to the very large TPA cross section near 4.2 eV, the correlation is clearly with state S_2, as was expected from Figure 12. We emphasize that the level of theory applied is important for these predictions.

Since the calculated spectra for $Ag_{31}(SCH_3)_{19}$ using the CAMB3LYP functional are more accurate than the results with any other functional, our discussion of the solvation effects on this system will be limited to CAMB3LYP. In the calculations on $Ag_{31}(SCH_3)_{19}$, the effect of inclusion of the PCM solvation model on the peak absorption energy is small, with a red shift of ∼0.08 eV due to the solvent. The effect of using the PCM for the geometry optimization is small, with a small average decrease in the Ag−Ag bond lengths, and a small average increase in the Ag−S bond lengths. From the insight gained from the TDDFT calculation with PCM for the gas-phase geometry, we can attribute ∼30% of the red shift to the structure change and ∼70% to the use of the PCM solvation model in the TDDFT response calculation. The effect of the solvation model on the intensity is more significant, with the PCM calculation yielding a peak extinction coefficient about twice that obtained in the gas-phase calculation.

The effect of the solvent model inclusion on the absorption spectra of $Ag_{15}(SCH_3)_{11}$ seems more significant since the shape of the measured absorption spectra is much better emulated when the solvation model is used. The best functional for this system is not as obvious, but careful analysis favors the PBE0 functional. The steep rise of the PCM spectra compared to the gas-phase data can be mainly attributed to the much larger oscillator strength ($f = 0.31$) of the most intense absorption state at 2.55 eV, compared to the most intense state in the gas-phase calculation (2.51 eV, $f = 0.09$). Thus, for both systems, the biggest effect of the solvation model is the increase in intensity for the most prominent absorption state.

CONCLUSIONS

Prediction of OPA spectra in comparison with available experimental data for silver nanoclusters has shown that, for the OPA of $[Ag_{44}(SR)_{30}]^{4-}$, the B3LYP functional performed the best, with acceptable performance from SAOP and mCAM, while for $Ag_{14}(SR)_{12}(PR'_3)_8$, good agreement was obtained only

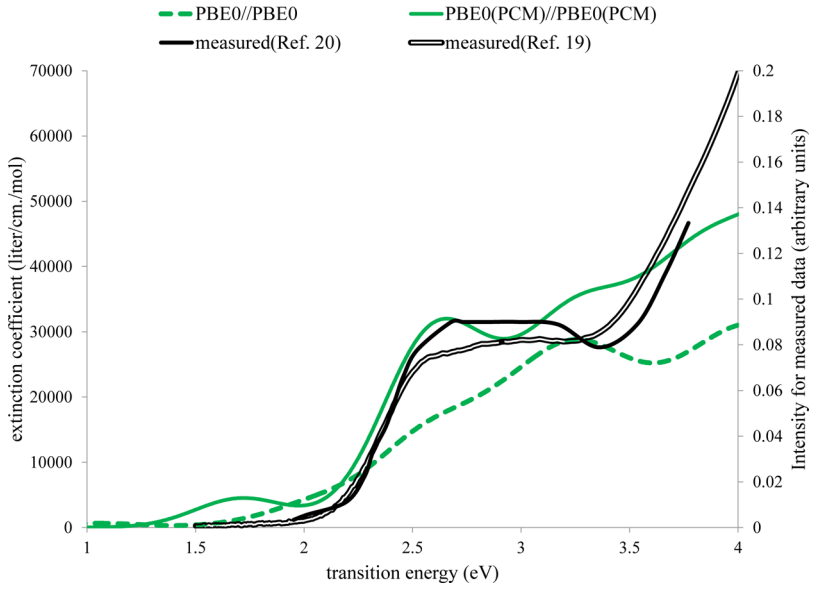

Figure 11. Linear absorption of $Ag_{15}(SR)_{11}$. Our calculated spectra used R = CH_3 and a line width of 0.5 eV. The measured results[19,20] had SR = glutathione.

DOI: 10.1021/acs.jpca.5b09623
J. Phys. Chem. A 2016, 120, 507−518

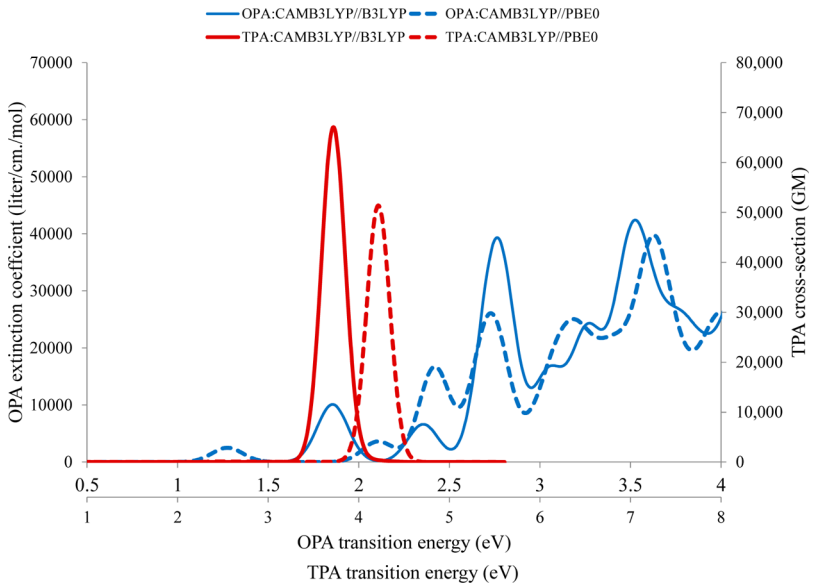

Figure 12. OPA and TPA of $Ag_{15}(SR)_{11}$, with the TPA transition energies plotted double scale of the OPA transition energies. Line width is 0.2 eV for OPA and 0.3 eV for TPA.

with the LB94 and SAOP functionals. For the Ag_{31}/Ag_{32} systems, excellent results were obtained with the CAMB3LYP functional, while for the Ag_{15} system, good results were obtained with the PBE0 functional and fair results were obtained with B3LYP and mCAMB3LYP. Our results indicate that using PBE for the prediction of the OPA spectra of silver clusters may lead to erroneous results. Note that structure prediction is still a challenge for silver nanoclusters, as recently pointed out by Wickramasinghe et al.[54]

Indeed, we note that accurate prediction of OPA is important for suppositions on the spectral range for TPA enhancement because of the sensitivity to the excitation energies. The OPA spectrum of the Ag_{44} system is largely independent of the specific thiolate ligand, likely due to the isolation of the inner icosahedral shell of silver atoms from the thiolate groups. We found that the Ag_{44} and Ag_{14} systems have significant spherical symmetry and follow the superatom rule for stability and even for optical properties. Calculations on the Ag_{44} and Ag_{15} systems predict large TPA, while the Ag_{14} system was found to have a small TPA over the range calculated but may have large TPA at higher energies where resonant enhancement may play a bigger role. The Ag_{31} system, which is predicted to have a modest TPA cross section of nearly 700 GM at a transition energy near 2.6 eV, likely has a much larger TPA cross section at a transition energy closer to 5 eV, due to resonance enhancement. Finally, it is interesting to note that, while prediction of TPA for these materials is a challenge due to the importance of resonance enhancement and its sensitivity to excitation energies, our calculations indicate large TPA for the less symmetrical Ag_{31}/Ag_{32} and Ag_{15} nanoclusters.

■ ASSOCIATED CONTENT

Supporting Information

The Supporting Information is available free of charge on the ACS Publications website at DOI: 10.1021/acs.jpca.5b09623.

Bond lengths in the Ag_{14} nanocluster, Cartesian coordinates for the Ag_{31}, Ag_{32}, and Ag_{15} systems, linear absorption spectra of the Ag_{44} and Ag_{15} systems with additional functionals, resonance enhancement factor for the Ag_{44} nanocluster as a function of transition energy for TPA-allowed states, and the TPA cross-section for each TPA-allowed state plotted versus the resonance enhancement factor τ for the Ag_{31} and Ag_{15} systems. (PDF)

■ AUTHOR INFORMATION

Corresponding Authors

*E-mail: paul.day.4.ctr@us.af.mil. (P.D.)
*E-mail: ruth.pachter@us.af.mil. (R.P.)

Notes

The authors declare no competing financial interest.

■ ACKNOWLEDGMENTS

We gratefully acknowledge support by the Air Force Office of Scientific Research and computer time and helpful support from the Air Force Research Laboratory DOD Supercomputing Resource Center.

■ REFERENCES

(1) Kim, B. H.; Hackett, M. J.; Park, J.; Hyeon, T. Synthesis, Characterization, and Application of Ultrasmall Nanoparticles. *Chem. Mater.* **2014**, *26*, 59−71.
(2) Ramakrishna, G.; Varnavski, O.; Kim, J.; Lee, D.; Goodson, T. Quantum-Sized Gold Clusters as Efficient Two-Photon Absorbers. *J. Am. Chem. Soc.* **2008**, *130*, 5032−5033.
(3) Ramakrishna, G.; Varnavski, O.; Kim, J.; Lee, D.; Goodson, T. Nonlinear Optical Properties of Quantum Sized Gold Clusters. *Proc. SPIE* **2008**, *7049*, 70490L.
(4) Polavarapu, L.; Manna, M.; Xu, Q.-H. Biocompatible Glutathione Capped Gold Clusters as One- and Two-Photon Excitation Fluorescence Contrast Agents for Live Cells Imaging. *Nanoscale* **2011**, *3*, 429−434.
(5) Philip, R.; Chantharasupawong, P.; Qian, H.; Jin, R.; Thomas, J. Evolution of Nonlinear Optical Properties: From Gold Atomic Clusters to Plasmonic Nanocrystals. *Nano Lett.* **2012**, *12*, 4661.
(6) Russier-Antoine, I.; Bertorelle, F.; Vojkovic, M.; Rayane, D.; Salmon, E.; Jonin, C.; Dugourd, P.; Antoine, R.; Brevet, P.-F. Non-Linear Optical Properties of Gold Quantum Clusters. The Smaller the Better. *Nanoscale* **2014**, *6*, 13572−13578.
(7) Day, P. N.; Nguyen, K. A.; Pachter, R. Calculation of One- and Two-Photon Absorption Spectra of Thiolated Gold Nanoclusters using

Time-Dependent Density Functional Theory. *J. Chem. Theory Comput.* **2010**, *6*, 2809−2821.
(8) Knoppe, S.; Hakkinen, H.; Verbiest, T. Nonlinear Optical Properties of Thiolate-Protected Gold Clusters: A Theoretical Survey of the First Hyperpolarizabilities. *J. Phys. Chem. C* **2015**, *119*, 27676−27682.
(9) Patel, S. A.; Richards, C. I.; Hsiang, J.-C.; Dickson, R. M. Water-Soluble Ag Nanoclusters Exhibit Strong Two-Photon-Induced Fluorescence. *J. Am. Chem. Soc.* **2008**, *130*, 11602−11603.
(10) Zheng, K.; Yuan, X.; Goswami, N.; Zhang, Q.; Xie, J. Recent Advances in the Synthesis, Characterization, and Biomedical Applications of Ultrasmall Thiolated Silver Nanoclusters. *RSC Adv.* **2014**, *4*, 60581−60596.
(11) Desireddy, A.; Conn, B. E.; Guo, J.; Yoon, B.; Barnett, R. N.; Monahan, B. M.; Kirschbaum, K.; Griffith, W. P.; Whetten, R. L.; Landman, U.; Bigioni, T. P. Ultrastable Silver Nanoparticles. *Nature (London, U. K.)* **2013**, *501*, 399−402.
(12) Conn, B. E.; Desireddy, A.; Atnagulov, A.; Wickramasinghe, S.; Bhattarai, B.; Yoon, B.; Barnett, R. N.; Abdollahian, Y.; Kim, Y. W.; Griffith, W. P.; Oliver, S. R. J.; Landman, U.; Bigioni, T. P. M_4Ag_{44}(p-MBA)$_{30}$ Molecular Nanoparticles. *J. Phys. Chem. C* **2015**, *119*, 11238−11249.
(13) Yang, H.; Wang, Y.; Huang, H.; Gell, L.; Lehtovaara, L.; Malola, S.; Hakkinen, H.; Zheng, N. All-Thiol-Stabilized Ag_{44} and $Au_{12}Ag_{32}$ Nanoparticles with Single-Crystal Structures. *Nat. Commun.* **2013**, *4*, 2422.
(14) Harkness, K. M.; Tang, Y.; Dass, A.; Pan, J.; Kothalawala, N.; Reddy, V. J.; Cliffel, D. E.; Demeler, B.; Stellacci, F.; Bakr, O. M.; McLean, J. A. $Ag_{44}(SR)_{30}^{4-}$: A Silver−Thiolate Superatom Complex. *Nanoscale* **2012**, *4*, 4269−4274.
(15) Yang, H.; Lei, J.; Wu, B.; Wang, Y.; Zhou, M.; Xia, A.; Zheng, L.; Zheng, N. Crystal Structure of a Luminescent Thiolated Ag Nanocluster with an Octahedral Ag_6^{4+} Core. *Chem. Commun.* **2013**, *49*, 300−302.
(16) Gell, L.; Lehtovaara, L.; Häkkinen, H. Superatomic S^2 Silver Clusters Stabilized by a Thiolate−Phosphine Monolayer: Insight into Electronic and Optical Properties of $Ag_{14}(SC_6H_3F_2)_{12}(PPh_3)_8$ and $Ag_{16}(SC_6H_3F_2)_{14}(DPPE)_4$. *J. Phys. Chem. A* **2014**, *118*, 8351−8355.
(17) Joshi, C. P.; Bootharaju, M. S.; Bakr, O. M. Tuning Properties in Silver Clusters. *J. Phys. Chem. Lett.* **2015**, *6*, 3023−3035.
(18) Pawlicki, M.; Collins, H. A.; Denning, R. G.; Anderson, H. L. Two-Photon Absorption and the Design of Two-Photon Dyes. *Angew. Chem., Int. Ed.* **2009**, *48*, 3244−3266.
(19) Ashenfelter, B. A.; Desireddy, A.; Yau, S. H.; Goodson, T.; Bigioni, T. P. Fluorescence from Molecular Silver Nanoparticles. *J. Phys. Chem. C* **2015**, *119*, 20728−20734.
(20) Bertorelle, F.; Hamouda, R.; Rayane, D.; Broyer, M.; Antoine, R.; Dugourd, P.; Gell, L.; Kulesza, A.; Mitric, R.; Bonacic-Koutecky, V. Synthesis, Characterization and Optical Properties of Low Nuclearity Liganded Silver Clusters. Ag31(SG)19 and Ag15(SG)11. *Nanoscale* **2013**, *5*, 5637−5643.
(21) Nguyen, K. A.; Day, P. N.; Pachter, R. The Performance and Relationship among Range-Separated Schemes for Density Functional Theory. *J. Chem. Phys.* **2011**, *135*, 074109.
(22) Rumi, M.; Ehrlich, J. E.; Heikal, A. A.; Perry, J. W.; Barlow, S.; Hu, Z.; McCord-Maughon, D.; Parker, T. C.; Rockel, H.; Thayumanavan, S.; Marder, S. R.; Beljonne, D.; Bredas, J.-L. Structure-Property Relationships for Two-Photon Absorbing Chromophores: Bis-donor diphenylpolyene and Bis(styryl)benzene Derivatives. *J. Am. Chem. Soc.* **2000**, *122*, 9500−9510.
(23) Sutherland, R. L. *Handbook of Nonlinear Optics;* Marcel Dekker, Inc: New York, 1996.
(24) Day, P. N.; Nguyen, K. A.; Pachter, R. TDDFT Study of One- and Two-Photon Absorption Properties: Donor-π-Acceptor Chromophores. *J. Phys. Chem. B* **2005**, *109*, 1803−1814.
(25) Day, P. N.; Nguyen, K. A.; Pachter, R. Calculation of Two-Photon Absorption Spectra of Donor-Acceptor Compounds in Solution Using Quadratic Response Time-Dependent Density Functional Theory. *J. Chem. Phys.* **2006**, *125*, 094103.
(26) Day, P. N.; Nguyen, K. A.; Pachter, R. Calculation of One-Photon and Two-Photon Absorption Spectra of Porphyrins Using Time-Dependent Density Functional Theory. *J. Chem. Theory Comput.* **2008**, *4*, 1094−1106.
(27) Becke, A. D. Density-Functional Exchange-Energy Approximation with Correct Asymptotic Behavior. *Phys. Rev. A: At., Mol., Opt. Phys.* **1988**, *38*, 3098−3100.
(28) Perdew, J. P. Density-Functional Approximation for the Correlation Energy of the Inhomogeneous Electron Gas. *Phys. Rev. B: Condens. Matter Mater. Phys.* **1986**, *33*, 8822.
(29) van Lenthe, E.; Baerends, E. J.; Snijders, J. G. Relativistic Total Energy Using Regular Approximations. *J. Chem. Phys.* **1994**, *101*, 9783.
(30) *ADF,* 2013.01 ed.; SCM, Theoretical Chemistry, Vrije Universiteit: Amsterdam, The Netherlands, 2013.
(31) Te Velde, G.; Bickelhaupt, F. M.; Baerends, E. J.; Fonseca Guerra, C.; Van Gisbergen, S. J. A.; Snijders, J. G.; Ziegler, T. Chemistry with ADF. *J. Comput. Chem.* **2001**, *22*, 931−967.
(32) Perdew, J. P.; Chevary, J. A.; Vosko, S. H.; Jackson, K. A.; Pederson, M. R.; Singh, D. J.; Fiolhais, C. Atoms, Molecules, Solids, and Surfaces: Applications of the Generalized Gradient Approximation for Exchange and Correlation. *Phys. Rev. B: Condens. Matter Mater. Phys.* **1992**, *46*, 6671−6687.
(33) Perdew, J. P.; Burke, K.; Ernzerhof, M. Generalized Gradient Approximation Made Simple. *Phys. Rev. Lett.* **1996**, *77*, 3865−3868.
(34) Adamo, C.; Barone, V. Accurate Excitation Energies from Time-Dependent Density Functional Theory: Assessing the PBE0Model for Organic Free Radicals. *Chem. Phys. Lett.* **1999**, *314*, 152−157.
(35) Hay, P. J.; Wadt, W. R. Ab initio Effective Core Potentials for Molecular Calculations. Potentials for K to Au Including the Outermost Core Orbitals. *J. Chem. Phys.* **1985**, *82*, 299.
(36) Frisch, M. J. T, G. W.; Schlegel, H. B.; Scuseria, G. E.; Robb, M. A.; Cheeseman, J. R.; Montgomery, Jr., J. A.; Vreven, T.; Kudin, K. N.; Burant, J. C.; Millam, J. M.; et al. *Gaussian 09,* B01 ed.; Gaussian, Inc: Wallingford, CT, 2009.
(37) Becke, A. D. Density-Functional Thermochemistry. III. The Role of Exact Exchange. *J. Chem. Phys.* **1993**, *98*, 5648−5652.
(38) Lee, C.; Yang, W.; Parr, R. G. Development of the Colle-Salvetti Correlation-Energy Formula into a Functional of the Electron-Density. *Phys. Rev. B: Condens. Matter Mater. Phys.* **1988**, *37*, 785−789.
(39) Vosko, S. H.; Wilk, L.; Nusair, M. Accurate Spin-Dependent Electron Liquid Correlation Energies for Local Spin Density Calculations: A Critical Analysis. *Can. J. Phys.* **1980**, *58*, 1200−1211.
(40) Stephens, P. J.; Devlin, F. J.; Chabalowski, C. F.; Frisch, M. J. Ab initio Calculation of Vibrational absorption and circular dichroism spectra using density functional force fields. *J. Phys. Chem.* **1994**, *98*, 11623−11627.
(41) Schmidt, M. W.; Baldridge, K. K.; Boatz, J. A.; Elbert, S. T.; Gordon, M. S.; Jensen, J. H.; Koseki, S.; Matsunaga, N.; Nguyen, K. A.; Su, S.; Windus, T. L.; Dupuis, M.; Montgomery, J. A. General Atomic and Molecular Electronic Structure System. *J. Comput. Chem.* **1993**, *14*, 1347−1363.
(42) A Molecular Electronic Structure Program. Dalton 2011 ed.; http://www.daltonprogram.org.
(43) Van Leeuwen, R.; Baerends, E. Exchange-Correlation Potential with Correct Asymptotic Behavior. *Phys. Rev. A: At., Mol., Opt. Phys.* **1994**, *49*, 2421.
(44) Schipper, P. R. T.; Gritsenko, O. V.; van Gisbergen, S. J. A.; Baerends, E. J. Molecular Calculations of Excitation Energies and (Hyper)polarizabilities with a Statistical Average of Orbital Model Exchange-Correlation Potentials. *J. Chem. Phys.* **2000**, *112*, 1344−1352.
(45) Zhao, Y.; Truhlar, D. G. The M06 Suite of Density Functionals for Main Group Thermochemistry, Thermochemical Kinetics, NoncovAlent Interactions, Excited States, and Transition Elements: Two nNew Functionals and Systematic Testing of Four M06-Class Functionals and 12 other Functionals. *Theor. Chem. Acc.* **2008**, *120*, 215−241.
(46) Yanai, T.; Tew, D. P.; Handy, N. C. A New Hybrid Exchange−Correlation Functional Using the Coulomb-Attenuating Method (CAM-B3LYP). *Chem. Phys. Lett.* **2004**, *393*, 51−57.

DOI: 10.1021/acs.jpca.5b09623
J. Phys. Chem. A 2016, 120, 507−518

(47) Nguyen, K. A.; Day, P. N.; Pachter, R. Effects of Solvation on One- and Two-Photon Spectra of Coumarin Derivatives: A Time-Dependent Density Functional Theory Study. *J. Chem. Phys.* **2007**, *126*, 094303.
(48) Stoll, H.; Fuentealba, P.; Schwerdtfeger, P.; Flad, J.; Von Szentpaly, L. V.; Preuss, H. Copper and Silver as One-Valence-Electron Atoms: CI Results and Quadrupole Corrections for Copper (Cu2), Silver (Ag2), Copper Hydride (CuH), and Silver Hydride (AgH). *J. Chem. Phys.* **1984**, *81*, 2732−2736.
(49) Dunning, T. H. J.; Hay, P. J. *Methods of Electronic Structure Theory;* Plenum Press: New York, 1977.
(50) Tomasi, J.; Mennucci, B.; Cammi, R. Quantum Mechanical Continuum Solvation Models. *Chem. Rev. (Washington, DC, U. S.)* **2005**, *105*, 2999−3093.
(51) Muniz-Miranda, F.; Menziani, M. C.; Pedone, A. DFT and TD-DFT Assessment of the Structural and Optoelectronic Properties of an Organic−Ag_{14} Nanocluster. *J. Phys. Chem. A* **2015**, *119*, 5088−5098.
(52) Goh, J.-Q.; Malola, S.; Hakkinen, H.; Akola, J. Silver Sulfide Nanoclusters and the Superatom Model. *J. Phys. Chem. C* **2015**, *119*, 1583−1590.
(53) Kumar, S.; Bolan, M. D.; Bigioni, T. P. Glutathione-Stabilized Magic-Number Silver Cluster Compounds. *J. Am. Chem. Soc.* **2010**, *132*, 13141−13143.
(54) Wickramasinghe, S.; Atnagulov, A.; Yoon, B.; Barnett, R. N.; Griffith, W. P.; Landman, U.; Bigioni, T. P. $M_3Ag_{17}(SPh)_{12}$ Nanoparticles and Their Structure Prediction. *J. Am. Chem. Soc.* **2015**, *137*, 11550−11553.

DOI: 10.1021/acs.jpca.5b09623
J. Phys. Chem. A 2016, 120, 507−518